Comparison of theoretical to experimental load bearing resistance of composite slabs

C.P.C. Bruwer
University of Johannesburg, Johannesburg, South Africa

ABSTRACT: Reinforced concrete structures can be strengthened by externally bonding steel plates to the concrete surface in tension creating a composite structural element. This paper compare the theoretically calculated flexural resistance of composite structural slabs to the experimentally tested results.

The test results of full scale experimental composite slabs are presented, loaded by either a point load at mid span or point loads at third spans mimicking a uniformly distributed load. The following variations in the in the composite slabs are considered: (1) number of bonded steel plates (2) width of the bonded steel plates (3) thickness of the bonded steel plates

1 INTRODUCTION

Reinforced concrete structural elements can be strengthened due to construction errors whereby too little reinforcement bars were placed in the concrete, corrosion of the reinforcing bars or due to an increase of the design load. A method for strengthening a reinforced concrete flexural member is to bond steel plates, as external reinforcement, to the tension face by means of epoxy. The advantages of this bonding technique are the relative simplicity of the application, the speed of construction and the small change in structural weight and size.

This paper compare the theoretically calculated flexural resistance to the experimentally tested flexural resistance as per HB 305-2008: Design handbook for RC structures retrofitted with FRP and metal plates: beams and slabs.

2 EXPERIMENTAL PROGRAMME

One way spanning reinforced concrete slabs are constructed for this research study, with sizes of 4800 mm long, 1000 mm wide and 125 mm thick.

The longitudinal reinforcement consist of five 12 mm diameter high yield reinforcement bars spaced at 200 mm intervals with a total cross sectional area of 565 mm^2. The cover to the longitudinal reinforcement bars is 25 mm. The transverse reinforcement is 12 mm diameter high yield bars spaced at 100 mm intervals. The 0.2% yield stress of the reinforcement bars is 534 MPa.

The concrete used for this research study is ready mixed, ordered with a compressive strength (f_{cu}) of 25 MPa. The concrete surface is prepared for bonding by removing the cement laitance by means of scabbling to expose the well-bonded large aggregate.

The plates to be bonded is of grade 350W mild steel, 4000 mm long terminating 250 mm short of the supports. The steel plate surface is prepared for bonding by means dry grit blasting to a white metal finish to obtain a 100–140 µm blast profile. The 0.2% yield stress of the steel plates is indicated in table 1.

Pro-Struct 618LV primer, which penetrate the concrete, is applied to establish good adhering between the concrete surface and the Pro-Struct 617NS non-sag epoxy which bond the steel plates to the concrete surface.

The slabs are simply supported at a 4500 mm spacing. Loading applied onto the slabs are by means of either a third-span line load (TSLL), indicated in figure 1, to mimic a uniformly distributed load, or a mid-span line load (MSLL) indicated in figure 2. Table 1 indicate the research specimens with the type of load applied, the number and size of steel plates, the concrete properties and the steel plate properties.

Figure 1: TSLL applied

Figure 2: MSLL applied

Table 1: Research specimens constructed

Slab Name	Type of Line Load	Number and Size of Bonded Steel Plate/s	Concrete Cube Strength (f_{cu})	Concrete Cylinder Strength	E- Modulus Concrete (E_c)	Concrete Tensile Strength (f_{ct})	Steel Plate Yield Stress (f_y)
		(mm)	(MPa)	(MPa)	(GPa)	(MPa)	(MPa)
Comp 1-T	TSLL	1, 110 x 6	24.70	19.76	35.00	2.19	461.00
Comp 2-T	TSLL	1, 110 x6	24.70	19.76	35.00	2.19	461.00
Comp 3-T	TSLL	1, 110 x 6	24.70	19.76	35.00	2.19	461.00
Comp 4-T	TSLL	2, 110 x 6	23.10	18.48	35.00	2.10	461.00
Comp 5-T	TSLL	2, 110 x 6	23.10	18.48	35.00	2.10	461.00
Comp 6-T	TSLL	2, 110 x 6	23.10	18.48	35.00	2.10	461.00
Comp 7-T	TSLL	1, 150 x 8	24.70	19.76	35.00	2.19	446.00
Comp 8-T	TSLL	1, 150 x 8	24.70	19.76	35.00	2.19	446.00
Comp 9-T	TSLL	2, 150 x 8	23.10	18.48	35.00	2.10	446.00
Comp 10-T	TSLL	2, 150 x 8	23.10	18. 48	35.00	2.10	446.00
Comp 1-M	MSLL	1, 110 x 6	24.70	19.76	35.00	2.19	461.00
Comp 2-M	MSLL	1, 110 x 6	23.10	18.48	35.00	2.10	461.00
Comp 3-M	MSLL	1, 110 x 6	30.60	24.48	37.00	2.53	461.00
Comp 4-M	MSLL	2, 110 x 6	24.70	19.76	35.00	2.19	461.00
Comp 5-M	MSLL	2, 110 x 6	23.10	18.48	35.00	2.10	461.00
Comp 6-M	MSLL	1, 150 x 8	24.70	19.76	35.00	2.19	446.00
Comp 7-M	MSLL	1, 150 x 8	30.60	24.48	35.00	2.53	446.00
Comp 8-M	MSLL	2, 150 x 8	24.70	19.76	35.00	2.19	446.00
Comp 9-M	MSLL	2, 150 x 8	24.70	19.76	35.00	2.19	446.00

3 DEBONDING MECHANISMS

The hinge design philosophy, based on the principle that the bonded plates terminate short of the point of contraflexure, is used for this research study and not the anchorage design philosophy which requires the bonded plates to end in an uncracked region, implying beyond the point of contraflexure.

The following debonding mechanisms are investigated.

3.1 *Intermediate crack (IC) debonding*

Intermediate crack debonding occur when flexural or flexural shear cracks in the reinforced concrete beam intercepts the bonded plate turning in the direction of the plate and join together.

Seracino et al. (2007) proposed equation 1 to determine the IC debonding resistance.

$$(P_{IC})_{pp} = \sqrt{\tau_f \delta_f} \sqrt{L_{per} E_p A_p} \text{ (N)} \quad (1)$$

Teng et al. (2002) proposed equation 2 to determine the IC debonding resistance.

$$\left[(P_{IC})_{pp}\right]_{EB} = \alpha_{EB} \beta_p b_p \sqrt{E_p t_p \sqrt{f'_c}} \quad (2)$$

The intermediate crack (IC) stress (σ_{IC}) is per equation 3.

$$(\sigma_{IC})_{beam} = \frac{(P_{IC})_{pp}}{A_p} \quad (3)$$

The intermediate crack (IC) strain (ε_{IC}) is per equation 4.

$$\varepsilon_{IC} = \frac{(\sigma_{IC})_{beam}}{E_p} \quad (4)$$

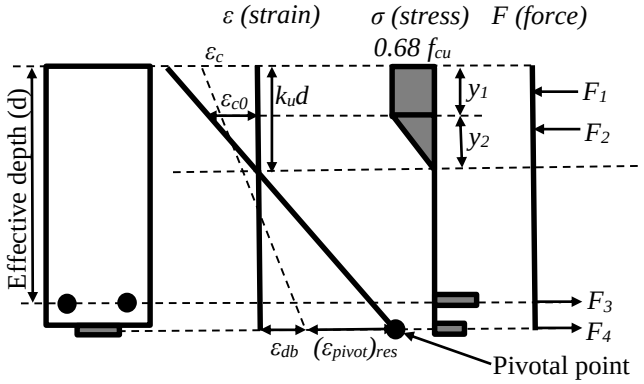

Figure 3: Flexural Analysis of an unpropped plated RC beam

Plating an unpropped concrete structural element, prior to an increase in the load, the plate strain is zero and the concrete strain adjacent to it is $(\varepsilon_{pivot})_{res}$, this strain difference always remain. When the composite structural element is loaded, the plate will debond at a strain of $\varepsilon_{db} = \varepsilon_{IC}$.and the strain in the adjacent concrete is $\varepsilon_{db} + (\varepsilon_{pivot})_{res}$. This is the pivotal point for the strain profile. The compressive strain in the concrete (ε_c) can be guessed and the depth of the neutral axis ($k_u d$) calculated. The concrete strain (ε_c) cannot exceed the maximum of 0.0035 and if it is the case, the pivotal point should be moved to $\varepsilon_c = 0.0035$ in the compression zone of the concrete.

From the determined strain profile in Figure 3 and knowing the concrete, reinforcement bars and bonded steel plate/s stress/strain relationships, the stress profile can be derived. The tensile strength of the concrete below the neutral axis is ignored due to the very large strains associated with failure.

Integrating the stresses over the areas in which they act gives the resultant forces (F) and their positions. The resultant of the longitudinal forces must sum to zero in order to establish longitudinal force equilibrium. This can be achieved by altering the strain in the concrete (ε_c). The moment capacity of the composite structural element can be derived from the longitudinal forces by taking moments about any convenient point.

3.2 *Critical Diagonal Crack (CDC) Debonding*

CDC debonding occur when an intermediate crack (IC), due to flexural or flexural/shear cracks, in the region of the support propagate due to an increase in the load and rigid body shear displacement occur. CDC debonding is usually evident in beams or slabs without shear stirrups. For reinforced concrete structural members with bonded longitudinal plates, the shear capacity is as follows:

$$V_{pl} = V_{uc} + \Delta V_{uc} \quad (5)$$

$$V_{uc} = v_c b_v d \quad (6)$$

The increase in the shear force capacity of the concrete structural element due to the bonded plate is:

$$\Delta Vuc = \sum_{i=1}^{n} \text{Pplate} \quad (7)$$

The longitudinal plates must, however, extend at least an anchorage length beyond the point of moment contraflexure, or to a region where the transverse shear force is very low. Due to the simply supported layout of the slabs being tested, the plates do not extend an anchorage length beyond the point of contraflexure, nor do they end in an area with a small shear force. Therefore the increase in the shear force capacity (ΔV_{uc}) does not apply to this research study.

3.3 *Plate End (PE) Debonding*

PE debonding occur due to to the curvature of a structural element. The curvature of a composite flexural member increases as the applied load increases, as the bonded plate tries to stay in contact with the surface of the structural element and at its original length, a moment (M_{plate}) and an axial force (P_{plate}) in the plate are induced. The stress concentration at the plate end result in interface cracks deveopling and spreading inwards causing PE debonding. PE debonding can be prevented by terminating the plate at the point of contraflexure (low curvature) or on the compression zone (near an internal support). The research specimens for this study was simply supported, therefore this prevention method is not applicable.

PE debonding (for externally bonded tension face plate) occur when the moment at the plate end reaches the capacity as per equation

$$\left[(M_{PE})_{tfp}\right]_{ch} = \frac{0.53(EI)_{cr.pl} f_{cb}}{0.474 E_p t_{tfp}} \quad (8)$$

3.4 *Interface shear stress debonding*

Interface shear stress or $\frac{\text{VAy}}{\text{Ib}}$ debonding occur if the interface shear stresses between the plate and the concrete are exceeded and the concrete fail due to tensile failure. According to Seracino et al. (2007) this failure mode occur very seldom and therefore was not considered for this research study.

4 RESULTS

The comparisons between the theoretically analyzed loads (P_{anal}) to the experimentally measured loads (P_{exper}) for the four debonding mechanisms is described below. Table 2 indicate the comparison between the theoretically analyzed loads (Seracino and Teng) to the experimentally measured loads for IC debonding.

Table 2: Comparison between the theoretically analyzed loads to the experimentally measured loads due to IC debonding using Seracino et al. (2007) and Teng et al. (2002) theories.

Slab Name	Type of Line Load	Number and Size of Bonded Steel Plate/s (mm)	Theoretically Analysed Load Seracino $(P_{anal})_{Ser}$ (kN)	Theoretically Analyzed Load Teng $(P_{anal})_{Ten}$ (kN)	Experimentally Measured Load (P_{exper}) (kN)	$(P_{exper})/(P_{anal})_{Ser}$	$(P_{exper})/(P_{anal})_{Ten}$
Comp 1-T	TSLL	1, 110 x 6	6.69	44.48	52.72	7.88	1.19
Comp 2-T	TSLL	1, 110 x 6	6.69	44.48	60.79	9.09	1.37
Comp 3-T	TSLL	1, 110 x 6	6.69	44.48	52.26	7.81	1.17
Comp 4-T	TSLL	2, 110 x 6	9.39	79.95	83.42	8.91	1.04
Comp 5-T	TSLL	2, 110 x 6	9.39	79.95	80.99	8.65	1.01
Comp 6-T	TSLL	2, 110 x 6	9.39	79.95	88.14	9.42	1.10
Comp 7-T	TSLL	1, 150 x 8	11.51	63.81	54.72	4.75	0.86
Comp 8-T	TSLL	1, 150 x 8	11.51	63.81	59.61	5.18	0.93
Comp 9-T	TSLL	2, 150 x 8	16.65	117.14	79.25	4.76	0.68
Comp 10-T	TSLL	2, 150 x 8	16.65	117.14	89.00	5.35	0.76
Comp 1-M	MSLL	1, 110 x 6	3.47	30.51	54.36	15.67	1.78
Comp 2-M	MSLL	1, 110 x 6	3.04	29.59	52.24	17.18	1.77
Comp 3-M	MSLL	1, 110 x 6	4.87	33.56	56.23	11.55	1.68
Comp 4-M	MSLL	2, 110 x 6	5.72	55.66	61.69	10.78	1.11
Comp 5-M	MSLL	2, 110 x 6	5.24	54.14	64.09	12.23	1.18
Comp 6-M	MSLL	1, 150 x 8	6.68	43.40	49.60	7.43	1.14
Comp 7-M	MSLL	1, 150 x 8	8.39	47.43	60.93	7.26	1.28
Comp 8-M	MSLL	2, 150 x 8	10.71	81.34	89.58	8.36	1.10
Comp 9-M	MSLL	2, 150 x 8	10.71	81.34	89.70	8.38	1.10

From table 2 above it is evident from comparing the experimentally measured load (P_{exper}) to the analyzed load (P_{anal}) that the Seracino et al. (2007) theory does not present as accurate results as the Teng theory.

Table 3 below compare the theoretically analyzed loads to the experimentally measured loads for PE debonding.

Table 3: Comparison between the theoretically analyzed loads to the experimentally measured loads due to PE debonding.

Slab Name	Type of Line Load	Number and Size of Bonded Steel Plate/s (mm)	Theoretically Analysed Load (P_{anal}) (kN)	Experimentally Measured Load (P_{exper}) (kN)	$(P_{exper})/(P_{anal})$
Comp 1-T	TSLL	1, 110 x 6	41.32	52.72	1.28
Comp 2-T	TSLL	1, 110 x 6	41.32	60.79	1.47
Comp 3-T	TSLL	1, 110 x 6	41.32	52.26	1.26
Comp 4-T	TSLL	2, 110 x 6	67.43	83.42	1.24
Comp 5-T	TSLL	2, 110 x 6	67.43	80.99	1.20
Comp 6-T	TSLL	2, 110 x 6	67.43	88.14	1.31
Comp 7-T	TSLL	1, 150 x 8	45.84	54.72	1.19
Comp 8-T	TSLL	1, 150 x 8	45.84	59.61	1.30
Comp 9-T	TSLL	2, 150 x 8	76.13	79.25	1.04
Comp 10-T	TSLL	2, 150 x 8	76.13	89.00	1.17
Comp 1-M	MSLL	1, 110 x 6	43.18	54.36	1.26
Comp 2-M	MSLL	1, 110 x 6	40.57	52.24	1.29
Comp 3-M	MSLL	1, 110 x 6	52.36	56.23	1.07
Comp 4-M	MSLL	2, 110 x 6	73.21	61.69	0.84
Comp 5-M	MSLL	2, 110 x 6	69.29	64.09	0.92
Comp 6-M	MSLL	1, 150 x 8	47.70	49.60	1.04
Comp 7-M	MSLL	1, 150 x 8	57.57	60.93	1.06
Comp 8-M	MSLL	2, 150 x 8	82.31	89.58	1.09
Comp 9-M	MSLL	2, 150 x 8	82.31	89.70	1.09

From table 3 above the experimentally measured load (P_{exper}) compared well to the theoretically analyzed load (P_{anal}) due to PE debonding.

Table 4 below identify the most likely debonding mechanism by finding the lowest analyzed point load.

Table 4: Determining the most likely failure mode by comparing the four debonding mechanisms.

Slab Name	Type of Line Load	Number and Size of Bonded Steel Plate/s	IC Debonding Seracino $(P_{anal})_{Ser}$	IC Debonding Teng $(P_{anal})_{Ten}$	PE Debonding (P_{anal})	Most Likely Debonding Mechanism
		(mm)	(kN)	(kN)	(kN)	
Comp 1-T	TSLL	1, 110 x 6	6.69	44.48	41.32	PE
Comp 2-T	TSLL	1, 110 x 6	6.69	44.48	41.32	PE
Comp 3-T	TSLL	1, 110 x 6	6.69	44.48	41.32	PE
Comp 4-T	TSLL	2, 110 x 6	9.39	79.95	67.43	PE
Comp 5-T	TSLL	2, 110 x 6	9.39	79.95	67.43	PE
Comp 6-T	TSLL	2, 110 x 6	9.39	79.95	67.43	PE
Comp 7-T	TSLL	1, 150 x 8	11.51	63.81	45.84	PE
Comp 8-T	TSLL	1, 150 x 8	11.51	63.81	45.84	PE
Comp 9-T	TSLL	2, 150 x 8	16.65	117.14	76.13	PE
Comp 10-T	TSLL	2, 150 x 8	16.65	117.14	76.13	PE
Comp 1-M	MSLL	1, 110 x 6	3.47	30.51	43.18	IC
Comp 2-M	MSLL	1, 110 x 6	3.04	29.59	40.57	IC
Comp 3-M	MSLL	1, 110 x 6	4.87	33.56	52.36	IC
Comp 4-M	MSLL	2, 110 x 6	5.72	55.66	73.21	IC
Comp 5-M	MSLL	2, 110 x 6	5.24	54.14	69.29	IC
Comp 6-M	MSLL	1, 150 x 8	6.68	43.40	47.70	IC
Comp 7-M	MSLL	1, 150 x 8	8.39	47.43	57.57	IC
Comp 8-M	MSLL	2, 150 x 8	10.71	81.34	82.31	IC
Comp 9-M	MSLL	2, 150 x 8	10.71	81.34	82.31	IC

From the above table it is evident that the analyzed PE debonding values (P_{anal}) is smaller than the IC debonding values $(P_{anal})_{Ten}$ for an applied TSLL (UDL) therefore PE occurs. When the MSLL is applied the IC debonding values $(P_{anal})_{Ten}$ is smaller than the PE debonding values (P_{anal}) therefore IC debonding occurs. The analytical observation above can be attributed to a higher mid span moment due to a MSLL than for a TSLL. Flexural or flexural/shear cracks would form in close proximity under a MSLL attributing to IC debonding. A TSLL yielding a smaller bending moment but larger curvature than the MSLL lead to PE debonding.

5 SUMMARY

IC debonding occur due to flexural or flexural/shear cracks forming in close proximity of the applied MSLL due to a high midspan moment. A larger curvature of the composite structural element occur when a TSLL (UDL) is applied therefore PE debonding would occur.

By comparing the experimentally measured load (P_{exper}) to the analyzed load (P_{anal}) for IC debonding, under a MSLL, the Teng et al. (2002) theory (average 10.98) yield better results than the Seracino et al. (2007) theory (average 1.35).

The experimentally measured load (P_{exper}) compared well to the theoretically analyzed load (P_{anal}) for PE debonding.

6 REFERENCES

HB 305-2008. Design handbook for RC structures retrofitted with FRP and metal plates: beams and slabs

Seracino, R.,Raizal Saifulnaz, M.R. & Oehlers, D.J. 2007. Generic debonding resistance of EB and NSM plate-to-concrete joints. Journal of Composites for Construction – ASCE, 11(1): 62-70

Teng, J.G., Chen, J.F., Smith, S.T. & Lam, L. 2002. FRP Strengthened RC Structures. Chichester, UK: Wiley.